Investigating Miscibility and Lithium Ion Transport in Blends of Poly(ethylene oxide) with a Polyanion Containing Precisely-Spaced Delocalized Charges

Nam Nguyen[1], Patrick Blatt[2], Kyoungmin Kim[2], Daniel T. Hallinan[2], and Justin G. Kennemur[1]**

[1] Department of Chemistry and Biochemistry, Florida State University, 95 Chieftan Way, Tallahassee, FL 32306, USA.

[2] Department of Chemical and Biomedical Engineering, Florida A&M University–Florida State University (FAMU-FSU) College of Engineering, 2525 Pottsdamer Street, Tallahassee, FL 32310, USA.

KEYWORDS. trifluoromethylsulfonimide, TFSI, ROMP, precision, polyanion, single-ion conductors, PEO.

For Table of Contents Use Only

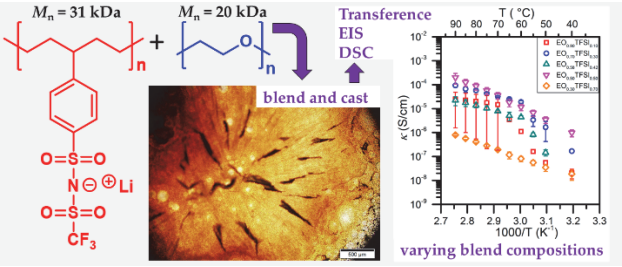

ABSTRACT

A novel precision single-ion conductor with phenylsulfonyl(trifluoromethylsulfonyl)imide lithium salt covalently bound to every fifth carbon of a polyethylene backbone, *p*5PhTFSI-Li, was synthesized via ring opening metathesis polymerization (ROMP) followed by post polymerization modification. The conversion of poly(4-phenylcyclopentene), bearing 94% sulfonate anions, to trifluoromethanesulfonimide (TFSI) anions was highly efficient (~90%) as determined by ^{19}F NMR analysis and corroborated through other spectroscopic methods. The flexible hydrocarbon backbone combined with a bulky TFSI anion led to an observable glass transition temperature of 199 °C even at these high levels of ionization. A high thermal stability up to 375 °C was also observed. Blending of *p*5PhTFSI-Li with poly(ethylene oxide) at various compositions was performed to investigate electrochemical performance and transference numbers with respect to the lithium electrode using a combination of impedance and polarization methods. At 90 °C and a 50:50 wt% blend composition, this system displayed the highest reported conductivity (2.00×10^{-4} S cm^{-1}) of a system with a demonstrated lithium-ion transference number near unity. Such performance is also atypical of single ion conductors produced through post-polymerization modification, which we attribute to the high yield of TFSI conversion. Investigations into the complex miscibility and phase behavior of these blends at various compositions was also probed by a combination of microscopy and differential scanning calorimetry, which is discussed with reference to computational predictions of how charge correlations affect polymer blend phase behavior.

INTRODUCTION

Continued advancements in energy dense battery storage, such as lithium ion batteries, benefit from fundamental studies aimed at exploring new synthetic materials, their phase behavior, and ultimately how these correlate to important ion transport parameters, such as conductivity and transference number.[1, 2, 3, 4, 5, 6] To this end, solid polymer electrolytes (SPE)s have received significant interest due to potential advantages, such as higher mechanical stability and enhanced safety in comparison to traditional liquid electrolytes, but typically at the expense of lower conductivity values.[7-10]

Research on SPEs has largely focused on aliphatic polyethers with dissolved small-molecule salts.[7-10] In particular, the poly(ethylene oxide) (PEO) and lithium bis(trifluoromethanesulfonyl)imide (LiTFSI) electrolyte has been rigorously studied due to its long unparalleled ionic conductivity (κ) among SPEs. The maximum conductivity of PEO doped with LiTFSI is ~10^{-3} S cm^{-1} at 90 °C.[11] Conversely, most liquid electrolytes have conductivities on the order of 10^{-2} to 10^{-1} S cm^{-1} at room temperature.[8, 11-14] A notable issue with dissolved salts is their propensity for the development of concentration gradients during cycling which is believed to exacerbate dendrite growth leading to cell failure.[15-20]

An alternative solution to dissolved salts is single ion conductors (SIC) which have been recently reviewed by Zhang et. al.[21] A SIC is defined as an electrolyte where only one ion, in this case lithium cations, is mobile during battery cycling. The restricted mobility of the anion can be achieved by covalently bonding it to the polymer backbone through post-polymerization modification or direct polymerization of charged monomers.[7, 21] SICs have cation transference numbers (t_+) typically >0.9, meaning most of the charge is carried by positive ions. As a point of comparison, binary SPEs (i.e. with dissolved salts) typically have $t_+ < 0.5$.[11] As a result of high

cation transference, SICs do not become polarized during cycling and concentration gradients across the electrolyte approach zero as $t_+ \rightarrow 1$. In a perfect SIC ($t_+ = 1$) concentration overpotential is completely avoided, leading to better battery efficiency and decreased internal resistance.[22, 23]

A recent approach to generating SIC SPEs is polymer blend electrolytes in which one blend component, the polysolvent, acts to enable lithium dissociation and transport while the other component, the polyanion, has anions covalently bound to the polymer backbone.[24] For clarity, these SPEs will be referred to as polymer blend electrolytes herein. In most cases, poly(ethylene oxide), PEO, is used as the polysolvent while the polyanion features large, charge delocalized anions. The utility of PEO as a polysolvent is two-fold: the ether oxygens facilitate lithium ion dissociation while the low glass transition temperature (T_g), typically reported as –60 °C, promotes a high degree of segmental motion for cation transport.[13, 25] For the polyanion, choosing large and delocalized anions serves to decrease the change in free energy upon dissociation of the cation/anion complex, and the negative charge is considered weakly coordinating. By blending the salient features of these two components, modularity in the ion to solvent ratio may be investigated without the need for synthesizing new materials each time. Research on polymer blend electrolytes has featured studies on a variety of anion moieties, which have generally increased in size with time while ionic conductivities have increased accordingly. Collectively, Armand, Balsara, Granados-Focil, Müller, Zhou and their respective coworkers have proven the ability of polymer blend electrolytes to compete with PEO/LiTFSI mixtures.[24, 26-30] Leading polymer blend electrolytes have exhibited conductivities on the order of 10^{-4} S cm^{-1} at 90 °C and transference numbers in excess of 0.9.[27, 28, 30]

Previously, we reported the ring opening metathesis polymerization (ROMP) of 4-phenylcyclopentene and its mild hydrogenation to produce a unique precision polymer that features a linear polyethylene backbone with a phenyl branch located at every 5th carbon.[31] The inherent flexibility supplied by four methylene units between each phenyl branch resulted in a lower T_g of ~17 °C when compared to polystyrene (~105 °C).[31, 32] We also showed that near quantitative sulfonation of this polymer was possible and, when neutralized with varying counter-cations (Li^+, Na^+, Cs^+), produced a new set of precision SICs that were water soluble and thermally stable.[33] The unique spacing of the polar sulfonate anions, coupled to the flexible non-polar hydrocarbon backbone, was later shown capable of self-assembling into nano-scale percolated ionic networks in the bulk state that exhibited Arrhenius conductivity behavior of Li ions up to 10^{-7} S cm^{-1} at 180 °C.[34] Furthermore, recent efforts to blend these materials with PEO revealed that they were miscible ($\chi_{eff} = -0.21$).[35] Moreover, the conductivity ($10^{-8} - 10^{-7}$ S cm^{-1} at 90 °C) was dependent on blend composition. The fraction of charge carried by Li ions ranged from 0.12 to 0.98 when traversing from mostly PEO to mostly SIC in the blend, respectively.[35] These investigations presented distinctive insights on a flexible alternative to polystyrene sulfonate (PSS) for understanding how SIC microstructure relates to properties. Inspired by the work of Meziane et al.,[30] who synthesized a TFSI-anchored polymer electrolyte, lithium poly[4-styrenesulfonyl(trifluoromethylsulfonyl)imide] (PSTFSILi), we envisioned that increasing the size and delocalization of the sulfonate anion into a TFSI-anchored derivative will improve the ionic conductivity while presenting further insight on these precise SICs for blending with PEO and investigating SPE behavior. In addition, the difference in polarity between sulfonate and TFSI ion chemistries will enable further insight into miscibility behavior between PEO and precise polyanions and its effect on lithium ion transport.[36]

EXPERIMENTAL

Synthesis of the precision SIC with phenylsulfonyl(trifluoromethylsulfonyl)imide-Li pendants. (*p*5PhTFSI-Li). For clarity herein, the nomenclature used to describe our precise polyanion will be *p*5PhX-Y, of which *p*5 stands for precise 5-carbon spacing, Ph stands for a phenyl group in direct connection to the backbone, and "X-Y" stands for type of chemistry on the *para* position of the phenyl group (e.g. sulfonic acid = S-H).

Synthesis of poly(4-phenylcyclopentene), followed by quantitative hydrogenation (*p*5Ph) and sulfonation (*p*5PhS-H) was performed in accordance with previous literature.[31, 33] The sulfonated polymer in the neutralized sodium form (*p*5PhS-Na) has a number average molar mass ($M_n \approx 21.5$ kg mol^{-1}) based on a degree of polymerization (N_n = 89) determined by size exclusion chromatography of the parent *p*5Ph using conventional column calibration against PS standards. Full details of the SEC characterizations are provided in the supporting information document. The degree of sulfonation (94%) was determined through titration (Supporting Information). The dispersity (Đ) of *p*5Ph is ~1.6 (Figure S2) and previous investigations revealed that the sulfonation procedure resulted in negligible degradation of the polymer.[33]

Following a modified procedure of Meziane et al.,[30] the *p*5PhS-Na was converted into the sulfonyl chloride derivative (*p*5PhS-Cl) through use of the Vilsmeier-Haack reagent produced from oxalyl chloride and a catalytic amount of dimethylformamide (Figure 1a). Due to its reactivity, the *p*5PhS-Cl was immediately converted to the lithium sulfonyl(trifluoromethylsulfonyl)imide derivative (*p*5PhTFSI-Li) through reaction with trifluoromethanesulfonamide. The resulting light brown polymer was collected (55.6% yield over both steps) and thoroughly dried under vacuum at 160 °C for 24 h prior to blending with PEO. Materials and full synthetic details can be found in the supporting information document.

Preparation of Polymer Blends for Differential Scanning Calorimetry (DSC). Blend compositions ranging from 90–10% (w/w) PEO (M_n = 20 kg mol^{-1}, Sigma-Aldrich) with *p*5PhTFSI-Li were prepared. For each blend, ~50 mg was obtained by dissolving measured amounts of *p*5PhTFSI-Li and PEO in a mixture of 80:20 volume ratio of acetonitrile (MeCN) and deionized water. The solutions were stirred for 24 h before being cast directly in aluminum DSC pans at 60 °C for 24 h on a temperature-controlled, level casting surface. The resulting sample filled DSC pans were dried *in vacuo* for 36 h at 160 °C and purged with Ar prior to hermetic sealing and characterization. Pure PEO was prepared as a control by employing the same method. All blend compositions were coded as EOxPhTFSIy in which EO represents PEO, PhTFSI represents *p*5PhTFSI-Li, and subscripts *x* and *y* represent the weight fraction of each component. The prepared blend compositions and cation to ethylene oxide molar ratios are shown in Table 1.

Table 1. DSC blend compositions

Sample[1]	Weight fraction of PEO	Cation to oxygen molar ratio ([Li^+]/[EO])
PEO	1	0
$EO_{0.90}PhTFSI0_{.10}$	0.9	0.013
$EO_{0.80}PhTFSI0_{.20}$	0.8	0.031
$EO_{0.70}PhTFSI_{0.30}$	0.7	0.051
$EO_{0.58}PhTFSI_{0.42}$	0.58	0.087
$EO_{0.50}PhTFSI_{0.50}$	0.5	0.13
$EO_{0.30}PhTFSI0_{.70}$	0.3	0.29
$EO_{0.10}PhTFSI_{0.90}$	0.1	1.1

[1] For sample IDs $EO_xPhTFSI_y$, the subscripts *x* and *y* represent the weight fraction of that component.

Differential Scanning Calorimetry (DSC) Experiments were conducted with a TA Q2000 equipped with an RC900 intracooler and operated under dry nitrogen gas. To investigate glass transition temperature (T_g) of blend compositions, samples were heated from -90 °C to 215 °C at a rate of 30 °C min^{-1} and cooled from 215 °C to –90 °C at a rate of 100 °C min^{-1} three times. T_g was determined from the third heating scan. In order to investigate melting and crystallization behavior of blends, they were equilibrated at 100 °C to erase thermal history before being cooled to –90 °C and reheated to 100 °C at a rate of 10 °C min^{-1}. Melting and crystallization temperature of PEO was determined upon heating and cooling cycles, respectively.

Polarized Optical Microscopy. The preparation of samples for optical microscopy was conducted in a similar fashion to how samples were prepared for DSC. Pure PEO, $EO_{0.90}PhTFSI_{0.10}$ and

$EO_{0.80}PhTFSI_{0.20}$ were cast on micro cover glasses from Ted Pella (22 x 22 mm) with the thickness between 0.16 and 0.19 mm. The samples were dried at 60 °C for 24 h and further dried under vacuum at 160 °C for another 36 h. Immediately prior to acquiring micrographs, samples were heated to 90 °C using a Linkam heating stage connected to a TMS94 temperature programmer and allowed to cooled to room temperature. Cooling was done passively by allowing the Linkam stage to reach room temperature which took approximately five minutes. Polarized optical micrographs were obtained using an Olympus BX51 optical microscope that was equipped with an Olympus type DP72 digital camera and analyzed using cellSens software.

Preparation of Blends for Ionic Conductivity and Transference Number Measurements. Polymer blends ranging in composition from pure PEO to 90 wt% *p*5PhTFSI-Li /10 wt% PEO were generated by combining calculated masses of PEO and *p*5PhTFSI-Li in borosilicate glass vials. Approximately 50 mg of each composition was measured. Each blend was then dissolved in approximately 250 μL of solution and stirred overnight at room temperature. Due to variations in blend solubility at varying composition, a two solvent system was employed and details are provided in Table S1. The first group, consisted of *p*5PhTFSI-Li rich blends (greater than 42 wt% *p*5PhTFSI-Li) that required a water co-solvent to enable the formation of a homogenous solution. As such, the aqueous group blends were dissolved in an 80:20 volume ratio of acetonitrile to water solvent. Conversely, the nonaqueous group (less than 42 wt% p5PhTFSI-Li) was formed using pure acetonitrile as a solvent. Both groups were cast on glass slides at 60 °C for 48 h, with the aqueous group casted in an air atmosphere while the nonaqueous group was cast in an argon-filled glovebox. Each blend was then collected in glass vials prior to being purged with argon and dried *in vacuo* for 36 h at 160 °C.

After drying, each blend electrolyte was incorporated into lithium symmetric cells for electrochemical characterization. Cell construction was completed in an argon-filled glovebox with O_2 and H_2O levels below 0.1 and 0.4 ppm, respectively. Electrolyte-filled Garolite spacer rings with 1/8 in. inner diameter were placed between lithium metal electrodes with diameter of 3/16 in. (MTI Corporation), and nickel tabs (TOB New Energy) were used as current collectors. Prior to cell assembly, the thickness of each electrolyte (160 – 420 μm) was measured for conductivity calculations. Each cell was vacuum sealed in laminated aluminum sheets (MTI Corporation) to avoid exposure to air during electrochemical characterization. Finally, each cell was annealed at 90 °C with small current densities of 0.02 mA/cm^2 being passed between electrodes to promote the formation of stable solid electrolyte interfaces for further testing. After this conditioning step, variation in the interfacial resistance of each unpolarized cell remained constant within $\pm 2\%$.

Electrochemical Impedance Spectroscopy. The ionic conductivity of each blend composition was determined by measuring each lithium symmetric cell with electrochemical impedance spectroscopy (EIS). An alternating voltage with peak amplitude of 10 mV was applied in a frequency range of 1 MHz to 100 mHz. Cells were given 1 h to return to electrochemical equilibrium between measurements. The EIS measurements were conducted from 40 to 90 °C, with three replications per temperature per cell. At least two cells of each composition were constructed and measured. Thermal equilibration was performed for 3 h after each temperature change.

Transference Number Measurements. The cationic transference number was determined using the potentiostatic polarization method. Each cell was polarized using chronoamperometry at 10 mV for 1 h enabling the determination of the initial and steady state currents. The initial and steady

state resistances were determined using EIS. At least three measurements were taken at 60 and 90 °C, each.

RESULTS AND DISCUSSION

A series of spectroscopic analyses was performed to confirm the successful synthesis and conversion of *p*5PhS-Na to *p*5PhTFSI-Li. Direct comparison of the ^{1}H NMR spectra (Figure 1b) in DMSO-d_6 reveals a downfield shift of the aryl protons from 7.48 and 6.96 ppm for *p*5PhS-Na to 7.63 and 7.11 ppm for *p*5PhTFSI-Li. We attribute this shift to the deshielding of these protons caused by the enhanced delocalization of the PhTFSI moiety. In addition, the ^{13}C NMR spectrum of *p*5PhTFSI-Li (Figure S5) reveals a unique quartet signal at 124–117 ppm which specifically arises from the splitting of the trifluoromethyl carbon nucleus with its three neighboring fluorine atoms.

With the installation of 3 equivalent fluorine atoms in the PhTFSI functionality, ^{19}F NMR provides an opportunity to quantitatively evaluate conversion. Figure 1c presents a stacked comparison of the ^{19}F NMR singlet signal of the $CF_3SO_2NH_2$ reagent used (–79.4 ppm) and *p*5PhTFSI-Li (–77.9 ppm). The polymer spectrum also confirms successful purification and removal of any unreacted trifluoromethanesulfonamide. The distinct resolution of these two signals allows $CF_3SO_2NH_2$ to be used as an internal standard, and a third ^{19}F NMR analysis was performed in DMSO-d_6 using a known mass of *p*5PhTFSI-Li spiked with a known mass of $CF_3SO_2NH_2$ (Figure S8). Comparative integration of these signals allows for determination of the approximate number of repeating units within the polymer bearing a PhTFSI functionality (~84%) (Supporting Information). Based on the 94% of repeating units that were originally sulfonated, this

translates to ~90% of the *p*5PhS-Na repeating units being successfully converted into the PhTFSI functionality.

Attenuated total reflectance infrared (ATR-IR) spectroscopy was also employed to observe the difference between *p*5PhS-Li and *p*5PhTFSI-Li (Figure 1d). Here we note that *p*5PhS-Na was converted to *p*5PhS-Li by ion exchange for a more accurate vibrational absorption comparison.[33] For the *p*5PhTFSI-Li, new strong signals at 1320 cm^{-1} and 1280 cm^{-1} appear and correspond to asymmetric stretching of O=S=O unique to the PhTFSI moiety that are not present in *p*5PhS-Li.[33, 37] In addition, the strong asymmetric stretch signal of C–F at 1190 cm^{-1} indicates the presence of CF_3.[37, 38] Other vibrational modes of SO_2 in sulfonamides are also detected at 1160 and 1087 cm^{-1}.[30, 38] Finally, the symmetric S–N stretch and S–N–S vibrations are observed at 790 and 745 cm^{-1}, respectively.[37] For comparison, an overlay of the IR spectra of *p*5PhTFSI-Li and LiTFSI salt is shown in Figure S21. While direct comparison of a crystalline solid salt to an amorphous polymer has some complications, the general peak profiles of both are in agreement. One exception is the CF_3 symmetric and asymmetric signals, which have increased in intensity in the salt, as expected, due to the presence of two of these groups. Additionally, many of the signals in the LiTFSI salt are shifted to slightly higher wavenumber (higher energy), which may be attributed to its crystalline form, but also to the presence of an additional CF_3 group and its inductive effect on vibrational energies versus the phenyl group on one side of the polyanion. Previous work has shown that when the LiTFSI salt is dissolved in an amorphous PEO matrix, many of the TFSI signals decrease in wavenumbers, consistent with what we are observing here.[38]

With confidence in the successful synthesis of *p*5PhTFSI-Li, other physical and thermal properties were investigated. While *p*5PhS-Na is insoluble in MeCN, *p*5PhTFSI-Li dissolves in MeCN readily and maintains DMSO and aqueous solubility. The *p*5PhTFSI-Li also adopts a

lighter brown color compared to the sulfonate version (Figure S9). Thermogravimetric analysis (TGA) determined a 5% mass loss decomposition temperature (T_d) of 375 °C under argon (Figure S7). DSC revealed an observable glass transition temperature (T_g) of 199 °C (Figure 1e). Therefore *p*5PhTFSI-Li has higher thermal stability and a lower T_g than previously observed for *p*5PhS-Li which was reported to have a T_d of 242 °C and no T_g observed up to 220 °C.[33] The reduction in T_g may be rationalized by the larger and more delocalized PhTFSI anion.[39] When comparing this T_g to its polystyrene counterpart, PSTFSILi, early reports indicate a range between 150–160 °C at high levels of TFSI functionalization.[30, 40] However, recent studies have shown that the T_g of PSTFSILi may be as high as 256 °C.[41-43] This discrepancy may be attributed to varying degrees of ionization and the drying process of PSTFSILi as incomplete removal of small molecules can plasticize and lead to a lower observed T_g. Here we note that we are confident in a highly dry sample prior to DSC analysis as evidenced by the absence of a water or other solvent signals (with the exception of DMSO from the NMR solvent) in the ^{1}H NMR spectrum shown in Figure 1b and Figure S4.

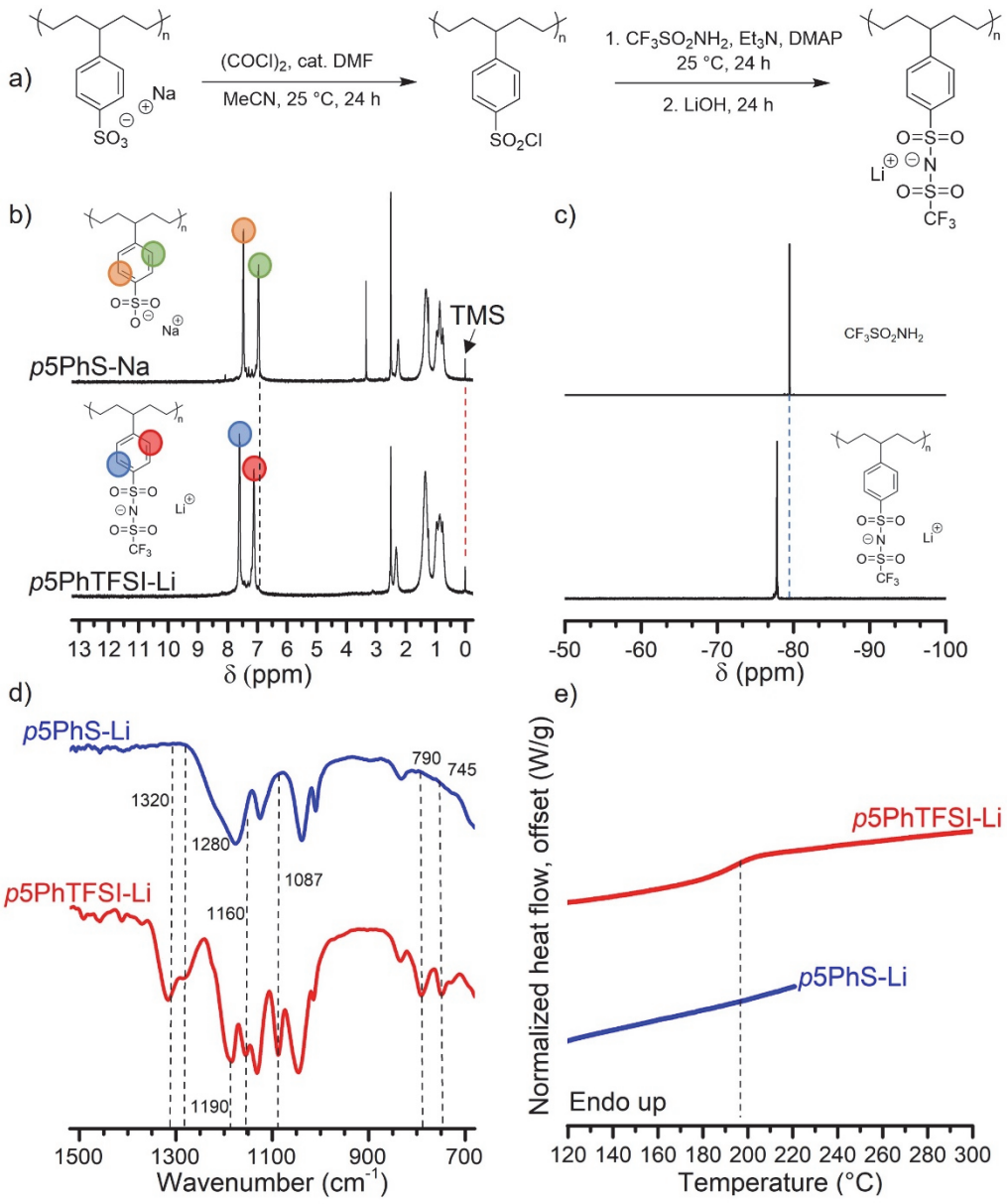

Figure 1. (a) Synthesis of p5PhTFSI-Li. (b) Stacked ^{1}H NMR spectra (600 MHz, DMSO-d_6, 25 °C) of *p*5PhS-Na (top) and *p*5PhTFSI-Li (bottom). Dashed lines are a guide to the eye showing downfield shifting of the aryl-H protons and the reference peak of tetramethylsilane (TMS) at 0.00 ppm. (c) Stacked ^{19}F NMR (375 MHz, DMSO-d_6, 25 °C) of $CF_3SO_2NH_2$ (top) and p5PhTFSI-Li (bottom). (d) Stacked ATR-IR of p5PhS-Li (top) and *p*5PhTFSI-Li (bottom). Dashed lines represent signals of interest to emphasize the change in vibrational absorption of *p*5PhTFSI-Li. (e)

DSC thermograms (2nd heating at 30 °C min^{-1}) of *p*5PhTFSI-Li (top) and *p*5PhS-Li (bottom). The vertical dashed line intersects the midpoint T_g of *p*5PhTFSI-Li at 199 °C.

The effect of blending on thermal transitions of the polymers was investigated with DSC. It is challenging to observe the T_g of semicrystalline PEO due to the weak signal that results from the minority amorphous component. Therefore, for T_g measurements of PEO and the blends, the sample was rapidly quenched from the amorphous state (cooling rate ~100 °C min^{-1}) and then heated at a ramp rate of 30 °C min^{-1}. The suppression of crystallization due to rapid quenching and the moderate heating rate were sufficient to observe T_g, as shown in Figure 2. Although not always the case (*vide infra*), it is generally accepted that a miscible, binary polymer blend has a single, composition-dependent T_g observed by DSC. Meanwhile, more than one T_g is typically observed if blends are immiscible and the T_g values of each blend component are sufficiently different. As shown in Figure 2, all blend compositions exhibit a single T_g between that of PEO (T_g = –48 °C) and *p*5PhTFSI-Li (T_g = 199 °C). This suggests that PEO and *p*5PhTFSI-Li are miscible in the amorphous state.

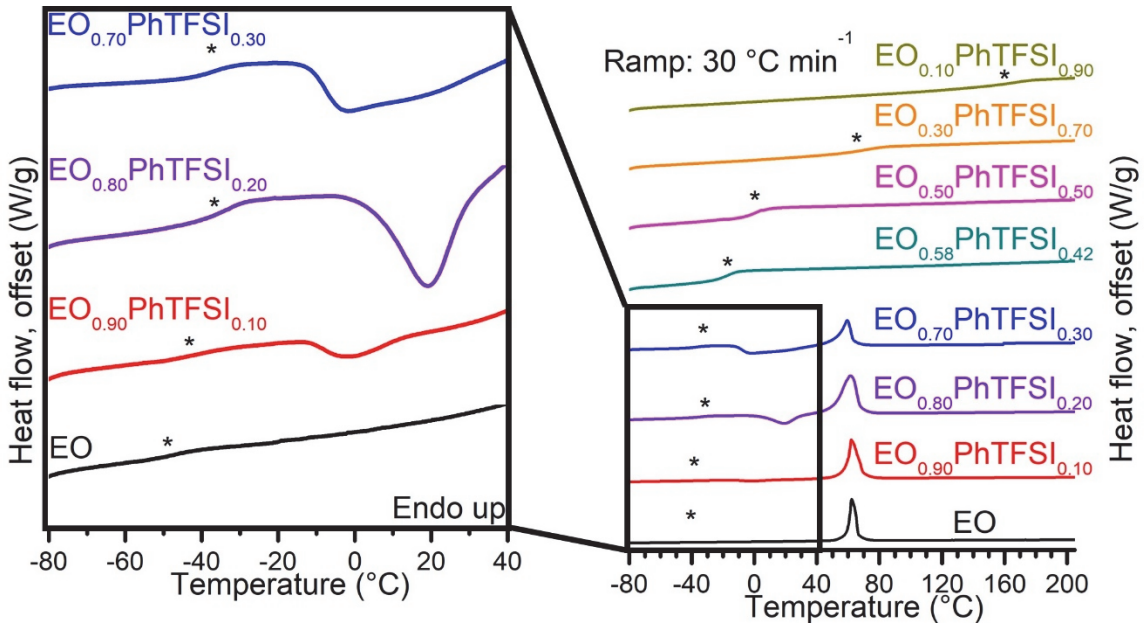

Figure 2. Offset DSC thermograms of $EO_xPhTFSI_y$ blends. (ramp rate = 30 °C min^{-1}, 3rd heating, endo up). The black box zooms in on the DSC thermograms of pure PEO and blends with up to 30 wt % PhTFSI from -80 °C to 40 °C for better T_g observation. Asterisks represent midpoint T_g value of blends.

As shown in Figure 3, the midpoint T_g values of each blend in Figure 2 exhibit negative deviation from the classic Fox equation. For blended components that contain more complex interactions, the Kwei equation (1) is often used to account for these specific interactions;[44]

$$T_{g,blend} = \frac{w_1 T_{g,1} + k w_2 T_{g,2}}{w_1 + k w_2} + q w_1 w_2 \qquad (1)$$

where w_1 and w_2 are weight fractions of PEO and *p*5PhTFSI-Li, respectively. $T_{g,1}$ and $T_{g,2}$ represent pure PEO and *p*5PhTFSI-Li homopolymer components, respectively, while k and q are fitting parameters. The best fit of the Kwei equation to the experimental data (by minimization of squared error) is shown in Figure 3. The values of q and k were –108.3 and 0.462, respectively. A small

value of k and a negative value of q indicate that the intermolecular interactions between PEO and *p*5PhTFSI-Li are predominated by self-associated interactions, which increases free volume of the blends and causes negative deviation of blend T_g from the Fox equation.[45]

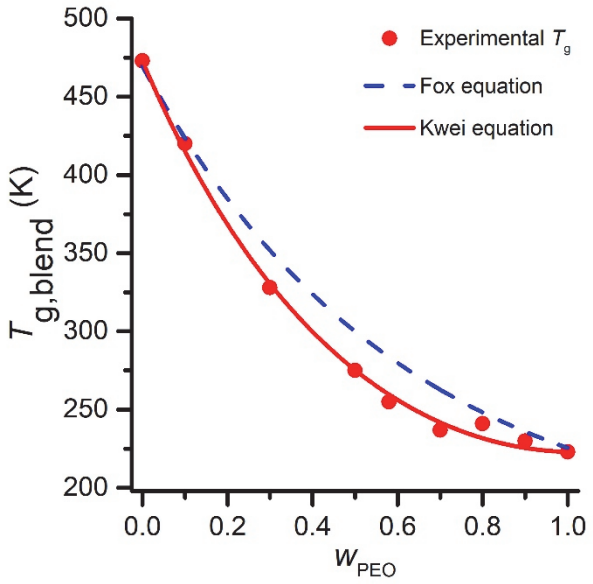

Figure 3. The T_g of $EO_xPhTFSI_y$ blends as a function of weight fraction of PEO, as well as fit of Kwei equation (red curve) and hypothetical T_g from Fox equation (dashed blue curve).

DSC of the blends was also used to examine how the crystalline phase of PEO is affected by the addition of a diluent such as *p*5PhTFSI-Li. For this purpose, a slower ramp rate of 10 °C min^{-1} was used. As shown in Figure 4a, endothermic melting peaks were observed in pure PEO (0 wt%) and blends up to 30 wt% of *p*5PhTFSI-Li. With increasing *p*5PhTFSI-Li content, the melting temperature (T_m) and the enthalpy of melting (ΔH_m) decreased and disappeared at 42 wt%. When observing thermograms upon cooling at 10 °C min^{-1}, an exothermic PEO crystallization peak is apparent in blends up to 30 wt% of *p*5PhTFSI-Li (Figure 4b). The lack of crystallization and melting peaks in blends of ≥42 wt% indicates that *p*5PhTFSI-Li interferes with the crystallization

of PEO at these compositions. In blends with ≤30 wt% *p*5PhTFSI-Li, the T_m of PEO is depressed with increasing *p*5PhTFSI-Li content, as shown in Figure 4c. This further corroborates the miscibility of the two polymers. T_m decreases from 63.7 °C for pure PEO to 62.8 °C at 10 wt% *p*5PhTFSI-Li and further decreased to 59.5 °C at 30 wt% *p*5PhTFSI-Li.

The ΔH_m values determined by DSC were used to determine the degree of PEO crystallinity in the blends according to equation (2):

$$X_c = \frac{\Delta H_m}{f \Delta H_m^0} \times 100 \qquad (2)$$

in which X_c is the degree of crystallinity per mass of PEO, ΔH_m^0 is the standard melting enthalpy of 100 % crystalline PEO, and f is the weight fraction of PEO in the blend. Due to a wide variety of reported values of ΔH_m^0 that range between 196 and 210 J g^{-1}, an average value of 203 J g^{-1} was taken to calculate the degree of crystallinity in PEO.[46-48] The degree of crystallinity reduced from 85% for pure PEO to 73% for $EO_{0.90}PhTFSI_{0.10}$ and further to 52% for $EO_{0.70}PhTFSI_{0.30}$ (Figure 4d). Blends containing 42 wt% *p*5PhTFSI-Li and above were amorphous. In our prior study observing blends of PEO with *p*5PhS-Li, it was found that PEO retained crystallinity regardless of *p*5PhS-Li content, which resulted in limited ionic conductivity at room temperature.[35] The disruption of crystallinity in this system can most likely be attributed to the larger TFSI anion, which is known to suppress PEO crystallinity.[49].

Addition of LiTFSI salt to PEO is known to suppress crystallinity more significantly than other lithium salts, as well as reduce crystallization kinetics.[35] Insight on the affect that various compositions of *p*5PhTFSI-Li has on the crystallization kinetics can be extracted from the observation of cold crystallization exotherms seen upon heating blends above T_g. This behavior manifests when the cooling rate is too fast to allow complete crystallization to occur below T_m and prior to reaching the T_g. Blends with 20 and 30 wt% *p*5PhTFSI-Li display cold crystallization

exotherms in Figure 2 and Figure 4a (see also Figure S12). No cold crystallization is seen for pure PEO or the 10 wt% blend, which suggests that crystallization kinetics are slowed by the *p*5PhTFSI-Li at 20–30 wt% which can be attributed to the smaller window between T_g and the crystallization temperature (T_c) of these blends. A similar trend has been shown for PEO-containing, miscible polymer blends such as PEO/poly(benzyl methacrylate) or PEO/poly(vinylphenol-*co*-methyl methacrylate) which also exhibit the onset of cold crystallization at 20 or 30 wt% of the amorphous component.[50, 51]

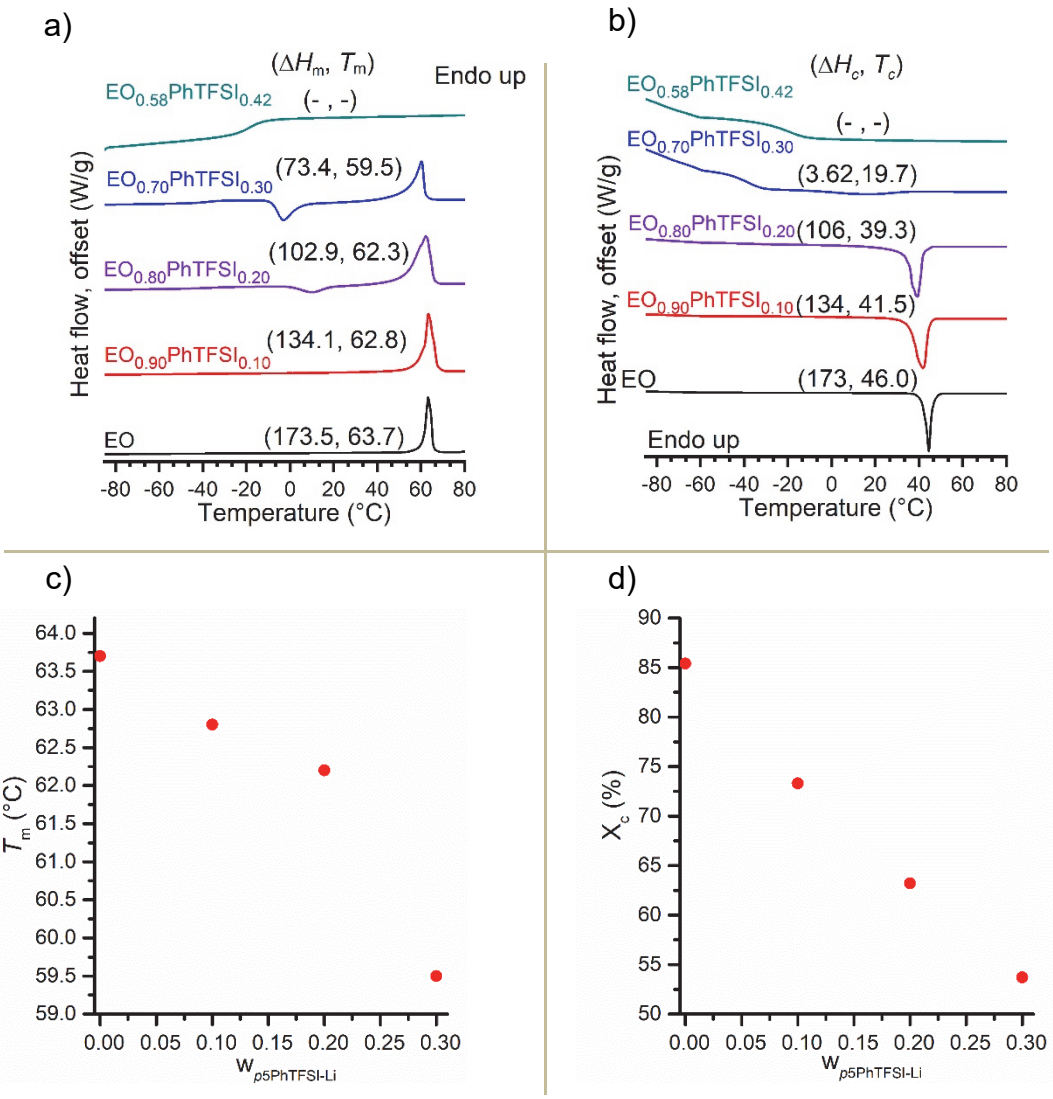

Figure 4. (a) Second heating DSC thermograms of blends of PEO with varying wt% of *p*5PhTFSI-Li up to 42 wt% (ramp rate = 10 °C min^{-1}, under N_2, endo up) and indicated values of ΔH_m (J g_{sample}^{-1}) and T_m (°C). (b) Cooling DSC thermograms of PEO after equilibrated at 100 °C with varying wt% of *p*5PhTFSI-Li up to 42 wt% (ramp rate = 10 °C min^{-1}, under N_2, endo up) and indicated values of ΔH_c (J g_{sample}^{-1}) and T_c (°C). c) T_m of PEO as a function of *p*5PhTFSI-Li weight fraction. (d) Degree of crystallinity per mass of PEO (X_c) as a function of *p*5PhTFSI-Li weight fraction. ΔH_m values of different compositions were taken upon second heating with ramp rate of 10 °C min^{-1} to calculate X_c.

The T_c of PEO upon cooling decreased with increasing *p*5PhTFSI-Li content up to 30 wt% (Figure 4b). Experimental T_c values were extrapolated to lower w_{PEO} using a quadratic fit (Figure 5), and the extrapolation intersects with the fitted Kwei equation at ~55 wt% of PEO. At this intersection, the T_g of the polymer blend is equal to T_c of PEO and the crystallization of PEO is inhibited by slow segmental mobility of the miscible blend. Below 55 wt% of PEO, crystallization is completely suppressed due to chain rigidity ($T_c < T_g$) and this is consistent with our DSC observations.

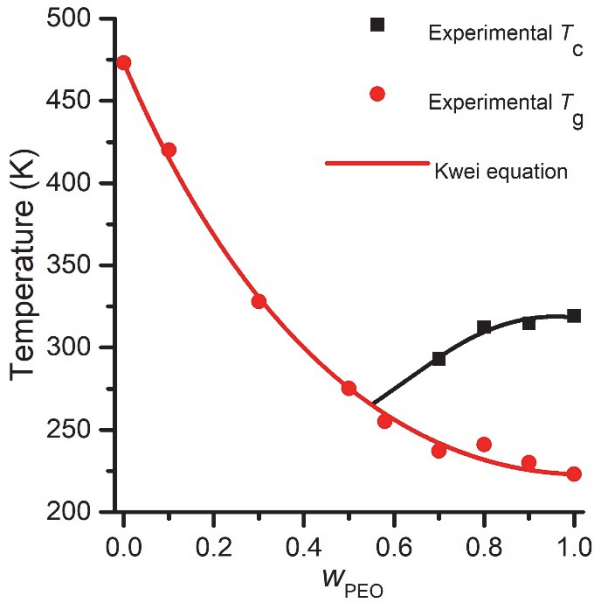

Figure 5. Crystallization temperature, T_c, of PEO (black squares) and glass transition temperature, T_g, of the blend (red circles) as a function of PEO weight fraction, w_{PEO}. The black curve is a quadratic fit to T_c and extrapolation intersects the fit of the Kwei equation (red curve) at the composition where crystallinity is completely absent (~55 wt% PEO).

For blends containing ≥42 wt% *p*5PhTFSI-Li, water had to be used as a cosolvent (20% v/v) along with acetonitrile to fully solubilize these compositions for blend casting. To ensure the use of this cosolvent did not affect the thermal properties, additional DSC analysis was performed on samples of $EO_{0.90}PhTFSI_{0.10}$ and $EO_{0.70}PhTFSI_{0.30}$ that were cast identically in both pure acetonitrile and with 20% v/v water in acetonitrile (Figures S10–S13). No significant differences in T_g or T_m and only slight differences in the cold crystallization peak shape were observed. This also corroborates that our drying protocols (36 h *in vacuo* at 160 °C) for the blends are sufficient with or without water as a cosolvent.

Overall, the DSC results suggest that PEO and *p*5PhTFSI-Li form a miscible blend. However, DSC alone has been shown inadequate for definitive conclusions of phase behavior. For example,

Lodge et al. revealed that miscible polymer blends, such as PEO/poly(methyl methacrylate), will exhibit two T_g values at midrange compositions (25–70%) owing to the Lodge-McLeish model and the large disparity of their homopolymer T_g values.[52] Oppositely, two components with similar T_g values, yet a high χ parameter, will display only one transition in DSC even while strongly segregated.[53] Our systems present a case where the blend components have very different T_g values yet show only one transition even in midrange compositions. However, for polymer electrolyte blends, the addition of electrostatic interactions can complicate the miscibility behavior. In fact, computational studies of polyelectrolyte/polymer blends reported by Sing et al. reveal that ion correlations enhance blend miscibility at all compositions when ion interactions are weak, but facilitate phase separation at low polyelectrolyte compositions when ion correlations are strong.[54-56] Upon looking at the DSC traces of our systems at low PhTFSI compositions, the weak T_g signals may not rigorously justify miscibility. Moreover, the relatively poor agreement with the Kwei equation at these compositions motivates a closer examination. Note the local maximum in Figure 5 at $w_{PEO} = 0.8$. Visual inspection of cast films of $EO_{90}PhTFSI_{10}$ and $EO_{80}PhTFSI_{20}$ reveal stark differences with the former exhibiting visual macrophase separation of dark PhTFSI-rich regions within the mostly colorless EO-rich matrix (Figure S24). Conversely, $EO_{80}PhTFSI_{20}$ appears homogenous and evenly colored (Figure S24). As seen in Figure 6b, polarized optical microscopy of $EO_{0.90}PhTFSI_{0.10}$ reveals regions that appear rich in *p*5PhTFSI-Li or PEO while optical microscopy of $EO_{0.80}PhTFSI_{0.20}$ in Figure 6c displays a much more homogenous appearance expected of a miscible composition. Furthermore, the large spherulites of PEO crystals in Figure 6b resemble those of pure PEO (Figure 6a) while much smaller spherulites are observed in Figure 6c. Here we note that the dark regions in the micrographs are likely to be voids within the film. These observations suggest that this system exhibits phase behavior of polyelectrolyte/polymer

blends with strong ion correlation, proposed by Sing et al. In other words, the $EO_{0.90}PhTFSI_{0.10}$ blend would be expected to fall inside the binodal line for phase miscibility. Therefore, we hypothesize strong ion correlation within the blends, and this is also corroborated by the data in Figure 3 and the Kwei parameters used.

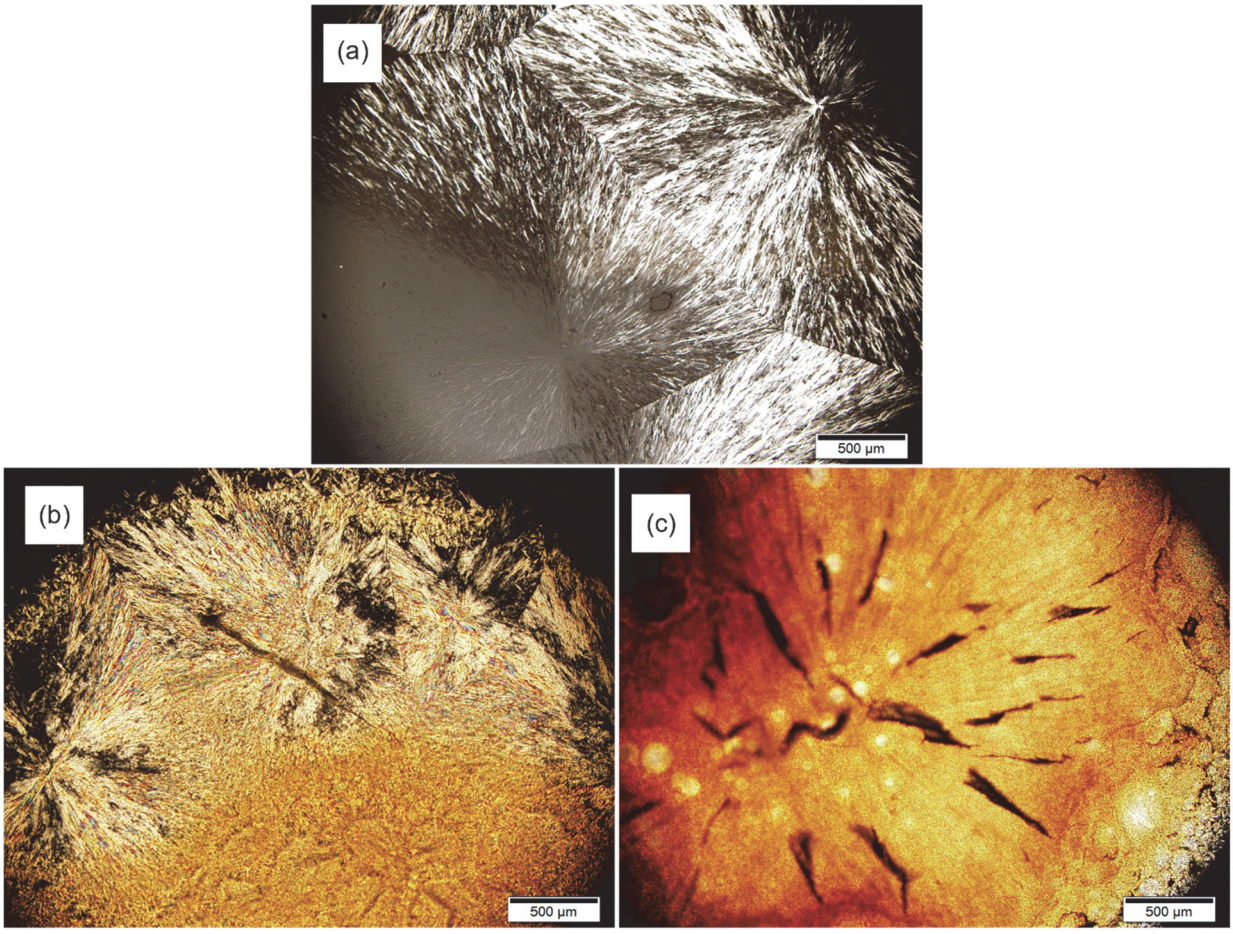

Figure 6. Optical microscope images of (a) Pure PEO (b) $EO_{0.90}PhTFSI_{0.10}$ and (c) $EO_{0.80}PhTFSI_{0.20}$

Electrochemical Characterization

As Figure 7a shows, ionic conductivities (κ) for PEO/*p*5PhTFSI-Li blends span a large range from 10^{-8} to 10^{-4} S cm^{-1} over the temperatures and compositions investigated. Melting has a

pronounced effect on conductivity in the semicrystalline blends. For $EO_{0.90}PhTFSI_{0.10}$, a significant increase in ionic conductivity was observed between 50 °C and 70 °C. Referencing Figure 4a, this increase in ionic conductivity coincides with the crystalline melting that begins at 50 °C and completes at 70 °C. Recognizing that ion conduction occurs primarily in the amorphous state, this increase in conductivity can be explained by the reduction of the crystalline phase, which increases the volume fraction of the conductive phase, reduces the tortuosity of conduction pathways, and increases segmental mobility.[11] Similar behavior has been observed in numerous other studies of transport in semicrystalline materials, including PEO-LiTFSI mixtures.[57] In the crystalline phase of PEO, ion transport is limited as the chain conformations are static inside the crystalline regions.[58, 59] With increasing *p*5PhTFSI-Li content, the degree of crystallinity decreases (see Figure 4d). This results in a smaller change in ionic conductivity with melting as *p*5PhTFSI-Li content is increased. At $EO_{0.70}PhTFSI_{0.30}$, the melting endotherm in Figure 4a is broader, such that some melting has occurred even at the lowest temperature at which conductivity was measured (40 °C).

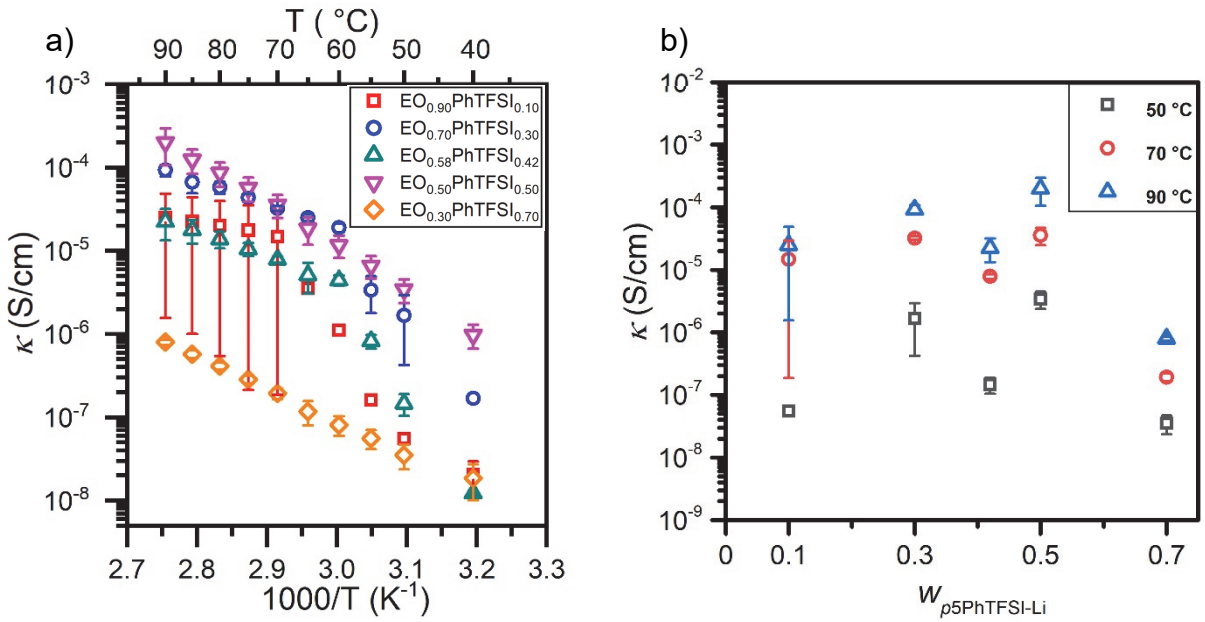

Figure 7. Ionic conductivity (κ) of $EO_xPhTFSI_y$ as a function of a) temperature and b) *p*5PhTFSI-Li weight fraction. Error bars represent one standard deviation of 3 measurements on at least 2 samples.

Interestingly, DSC indicates that $EO_{0.58}PhTFSI_{0.42}$ is fully amorphous (Figure 4a) despite a large increase in conductivity observed between 40 and 70 °C at this composition. At a scan rate of 10 °C min^{-1} observed by DSC, recrystallization kinetics are limited. As discussed in conjunction with Figure 5, crystallization is slow due to T_c being only slightly above T_g at this composition. Rather than requiring seconds to minutes, crystallization likely requires hours to days in $EO_{0.58}PhTFSI_{0.42}$. This phenomenon was observed in extended conductivity measurements at 40 °C over the course of days in $EO_{0.58}TFSI_{0.42}$, where the conductivity continued to decline over this period due to slow crystallization. $EO_{0.58}TFSI_{0.42}$ values reported in Figure 7 correspond to initial measurements after the cells were allowed to cool from 60 °C to 40 °C over the course of 1 hr. After this cooling period, subsequent isothermal measurements were taken every hour. The conductivity of the blend decreases with each of these subsequent measurements (Figure S19), suggesting slow isothermal crystallization is occurring. Due to conductivity data being collected on heating and samples spending hours at each temperature, more time was available for an equilibrium degree of crystallinity to be achieved in $EO_{0.58}PhTFSI_{0.42}$, which resulted in the melting signature being present in the conductivity data of Figure 7a. This is another example of how Li transport is sensitized to polymer structure, which can be another measure to detect crystallization.[60] It should

be noted that $EO_{0.58}PhTFSI_{0.42}$ was the only composition that showed this sensitivity to the heating protocol while all other compositions showed stable conductivities regardless of thermal history.

The truly amorphous blends, in which $T_c < T_g$ ($EO_{0.5}PhTFSI_{0.5}$ and $EO_{0.3}PhTFSI_{0.70}$), exhibit a single activation energy across the entire temperature range from 40 °C to 90 °C. In other words, if enough polyanion was added to entirely inhibit PEO crystallization, no step change was observed. This explains the lack of a drastic change in conductivity for the blends with *p*5PhTFSI-Li weight percentages greater than 42%.

The larger error bars produced from triplicate conductivity measurements on two samples of $EO_{0.90}PhTFSI_{0.10}$ in Figure 7 support the observation and conclusion of phase separation at this composition. Based on the colors of the pure components (PEO white and *p*5PhTFSI-Li light brown), visual inspection of Figure 6b indicates that there are phase regions more concentrated in each blend component for $EO_{0.90}PhTFSI_{0.10}$. Furthermore $EO_{0.80}PhTFSI_{0.20}$, shown in Figure 6c, appears miscible based on color uniformity. Therefore, the thermodynamic phase boundary occurs between 10 and 20 wt% *p*5PhTFSI-Li. The macroscopic phase separation below this critical polyanion composition causes non-uniform ion distribution and large variance in conductivity, as seen in Figure 7. At *p*5PhTFSI-Li >20 wt%, the error bars for conductivity were consistently smaller, which also supports the conclusion that these are miscible blends.

The conductivity data at three temperatures is presented again in Figure 7b as a function of *p*5PhTFSI-Li weight fraction to observe the effect of blend composition on ionic conductivity. Focusing on the data at 90 °C, where there is no complexity due to different degrees of crystallinity, it is clear that the blends with 30 to 50% *p*5PhTFSI-Li have the highest ionic conductivity, with the 50-50 blend being the best performing with an ionic conductivity of 2.00×10^{-4} S/cm. As reported in Table 1, these weight fractions correspond to Li^+:O mole ratios between 0.05 and 0.13,

which are the compositions at which PEO-LiTFSI (polymer-salt) mixtures have optimal ionic conductivity as well, with a value of 2×10^{-3} S/cm.[61, 62] The root cause of the local minimum in ionic conductivity at 42% *p*5PhTFSI-Li is unknown and subject to further investigation.

However, in the case of PEO/LiTFSI binary electrolytes, complex nonmonotonic relationships between salt concentration and transport parameters have been observed.[63-65] Such complex behavior has been attributed to competition between polymer segmental mobility, ion concentration, dissociation state, and interactions among components (ions and polymer). Specifically, polymer mobility, as represented by the segmental relaxation time, decreases monotonically with increasing salt concentration.[8] This is attributed to attractive associations between ether oxygens and lithium cations. Conversely, as more salt is added, more charge is available for conduction enabling higher overall conductivity. Moreover, the number of free, dissociated ions decreases above a limiting salt concentration, resulting in non-conductive neutral ion pair and less mobile charged ion clusters.[37] Considering that the cation and polysolvent are chemically identical to the binary PEO/LiTFSI electrolyte, the nonmonotonic behavior in Figure 7b could be due to similar effects. Additional work probing the relationship between polyanion concentration and *p*5PhTFSI-Li/PEO blend electrolyte properties is needed to prove that the concentration-dependent mechanisms occurring in binary polysolvent/salt mixtures are also present in polysolvent/polyanion blends. The fact that similar behavior has been observed with other salts, in PEO-containing block copolymers, and in single-ion conducting block copolymers, suggests that such complex behavior is dominated by the presence of PEO. [36, 66, 67]

In order to quantify the differing slopes apparent at high temperature in Figure 7a, the conductivity data between 70 and 90 °C was fit with the Arrhenius and Vogel-Fulcher-Tammann (VFT) models. Those results appear in Figure S22 and Tables S2 and S3. Due to the rather narrow

temperature range over which fits could be applied and the similar goodness of fit of the VFT and Arrhenius models, the activation energy from the Arrhenius fits were examined more closely in Figure S23. There is an apparent maximum in activation energy at the 50-50 blend, which exhibited the highest conductivity, followed by an apparent decrease in activation energy with increasing PEO content, from which might be inferred that PEO solvation facilitates ion mobility. However, the error bars of one standard deviation lead one to conclude that nothing quantitative can be concluded regarding the slope of conductivity in the fully amorphous samples.

The findings of this study reveal that PEO/*p*5PhTFSI-Li is competitive with state-of-the-art polymer-based SICs. For example, Zhou and coworkers studied PEO/lithium poly[(4-styrenesulfonyl)(fluorosulfonyl)imide] (LiPSFSI) which displayed a maximum conductivity of 5.3 $\times$ 10^{-5} S cm^{-1} at 90 °C,[27] while Meziane et al. reported PEO/PSTFSILi's maximum conductivity as 10^{-5} S cm^{-1} at 90 °C.[30] It should also be noted that PEO/*p*5PhTFSI-Li shows high conductivity due to the efficiency of our post–polymerization modification and suggests that polymerization of a charged monomer is not always needed to achieve high ionic functionalization.

As shown in Figure 8, transference numbers for the tested blends were all unity within experimental uncertainty. A t_+ value greater than one is possible, indicating that cations are migrating toward the cathode, as expected, and that some anions are also migrating toward the cathode (in the opposite direction to that expected based on their charge). This would indicate that the flow of Li ions, due to the applied electric field, is pulling polyanion chains along with them by electroneutrality. However, all error bars include unity indicating that these blends are, most probably, near perfect single-ion conductors. Limitations of the potentiostatic polarization method are numerous and should be acknowledged. The potentiostatic polarization method relies upon the assumption of dilute electrolytes and agreement between this method and more rigorous methods,

like galvanostatic polarization and the Newman Method declines in concentrated electrolytes.[68-70] Ion specific measurements, such as pulsed field gradient-nuclear magnetic resonance (PFG-NMR), could elucidate the physical cause of cation transference numbers greater than one, if in fact that is the case in these blends. The transference number values of PEO/*p*5PhTFSI-Li are the highest measured for a polymer-based SIC, to our knowledge. For instance, the previously mentioned PEO/LiPSFSI and PEO/PSTFSILi showed maximum transference numbers of 0.9 and 0.92 respectively.[27, 30, 59] Because the limiting current of an electrolyte is tied not only to ionic conductivity, but also to transference number,[23] a transference number of one and conductivity of 2.00×10^{-4} S/cm means that these blends are likely to exhibit battery cycling rates that are competitive with PEO/LiTFSI electrolytes.[24]

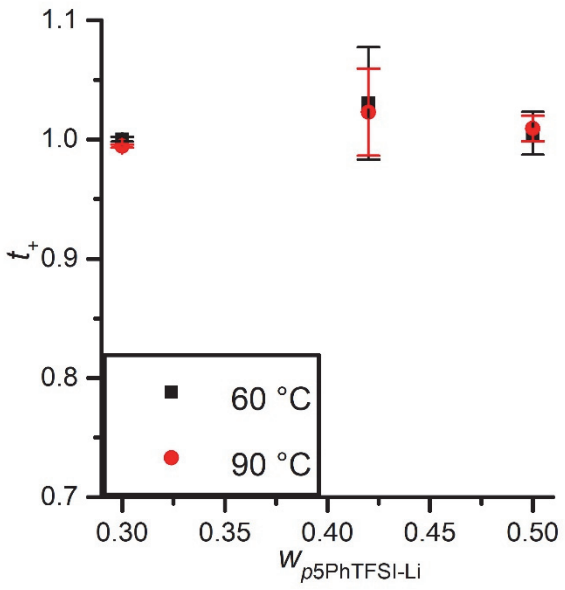

Figure 8. Cationic transference number (t_+) of 30, 42, and 50 wt% *p*5PhTFSI-Li blends at 60 °C and 90 °C. Error bars represent 1 standard deviation of at least 3 measurements on at least 2 samples.

In electrochemical cells such as batteries, conduction of only one ion is usually desired. This is the case in lithium-ion and lithium-metal batteries in which flux of lithium ions is the only flux that results in useful current. The ability of an electrolyte to conduct the ion of interest can be conveniently estimated as the product of the transference number of that ion and the overall ionic conductivity of the electrolyte. In Figure 9, this metric is used to compare our work with several polymer blend electrolytes whose transference number and conductivity have been reported. Also shown in Figure 9 is the canonical PEO/LiTFSI salt reference. A more rigorous prediction of limiting current of an electrolyte than $t_+\kappa$ can be determined using the dimensionless Newman number, Ne, as follows: $\kappa/(1+Ne)$. This accounts for thermodynamic non-ideality and has been determined by Balsara and coworkers.[13] This more rigorous reference is also shown in Figure 9. The $t_+\kappa$ value of the 50:50 blend in this work reaches the rigorous metric at 90 °C. Perhaps more interesting is the fact that the 50:50 blend in this work surpasses all other blend electrolytes at 40 °C. This appears to be due to the lack of a step change below 70 °C that occurs in the other blends because of PEO crystallization. The serendipitous depression of T_c to below T_g, which also remains below room temperature, appears to be an alternative approach to boost near-ambient polymer electrolyte conductivity. Other approaches that have achieved similar performance at and near room temperature include crosslinking PEO or incorporating PEO into a random or block copolymer.[21] Although the improvement over existing reports is modest, it stands out as the first study, to our knowledge, in which a post-polymerization modified polyelectrolyte blend has been

demonstrated able to compete with the state-of-the-art in single-ion conducting solid electrolytes. Moreover, it is the first report to our knowledge in which a truly unity transference number has been reported. Future work will explore the role that precision control of ion spacing along the polyelectrolyte backbone plays in blend electrolyte performance.

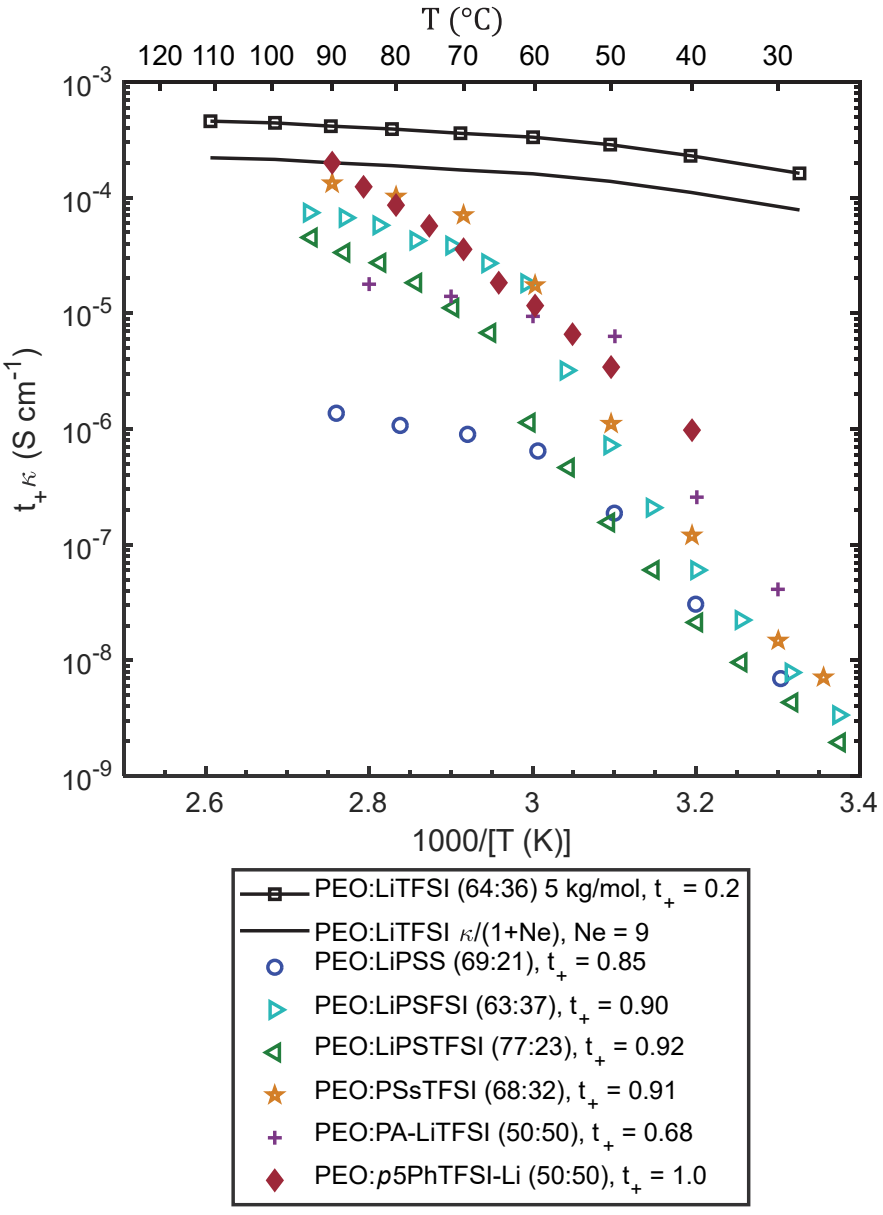

Figure 9. Arrhenius plot of lithium-ion conductivity, approximated as product of cation transference number and conductivity. Polymer blend electrolytes from this work (filled diamonds) and literature[24] (open symbols) are shown with polymer electrolyte reference, PEO/LiTFSI salt (curve through squares). Also shown is the more rigorous reference values of the polymer electrolyte reference (black curve) that accounts for thermodynamic non-ideality via the Newman number, Ne. Mass fractions of blends and mixtures are shown in legend. As shown in legend, the PEO reference has low molar mass, 5 kg/mol. Both conductivity and cation transference number have been reported for PEO blended with the following polyanions: LiPSS = lithium poly(4-styrene sulfonate), LiPSFSI = lithium poly[(4-styrenesulfonyl) (fluorosulfonyl)imide], LiPSTFSI = lithium poly[(4-styrenesulfonyl) (trifluoromethanesulfonyl)imide], LiPSsTFSI = poly[(4-styrenesulfonyl)(trifluorometh-yl(S-trifluoromethylsulfonylimino)sulfonyl)imide], PA-LiTFSI = lithium poly[(trifluoromethyl) sulfonyl acrylamide].

CONCLUSIONS

In this work a novel polyanion, *p*5PhTFSI-Li was blended with PEO whereupon a maximum ionic conductivity of 2.00×10^{-4} S cm^{-1} was measured at 90 °C for 50:50 wt% composition. These blends showed remarkable transference numbers near unity in combination with one of the highest ionic conductivities of a polymer blend electrolyte reported to date, even though the delocalized charges are spaced farther apart than in its PS counterpart. Visual inspection, optical microscopy, and DSC studies indicate that the blends are miscible at most *p*5PhTFSI-Li compositions. In addition to conductivity measurements, they also collectively indicate phase

coexistence at 10 wt % *p*5PhTFSI-Li, which was theoretically predicted for polymer blends with strongly correlated ions.[54, 56] This phenomenon will be investigated further in future work. The results herein demonstrate that continued fundamental studies on new synthetic materials, in combination with modular synthetic approaches (post polymerization modification) and formulation (blending), can be used to generate polymer electrolytes that are competitive with the state of the art.

The ease of synthesis and high ionic conductivity combined with innate benefits of SICs (dendrite suppression, rate capability, and energy efficiency) make *p*5PhTFSI-Li a promising polyanion for further study. Further work will focus on the effects of blend component molar mass and the implementation of *p*5PhTFSI-Li in systems with improved shear modulus which may further capitalize on the dendrite suppression offered by single-ion conductors. Toward this end, an examination of the mechanical properties of these blends and their performance in lithium batteries is worthwhile for future studies.

ASSOCIATED CONTENT

Supporting Information. Further synthetic details, procedures, characterization data, calculations, electrochemical measurements, and methods may be found in the Supporting Information document file that is available free of charge.

AUTHOR INFORMATION

Corresponding Authors

***Justin G. Kennemur** – *Department of Chemistry and Biochemistry, Florida State University, Tallahassee, Florida 32306-4390, United States;* orcid.org/0000-0002-2322-0386; Email: jkennemur@fsu.edu

***Daniel T. Hallinan** – *Department of Chemical and Biomedical Engineering, Florida A&M University–Florida State University (FAMU-FSU) College of Engineering, 2525 Pottsdamer Street, Tallahassee, Florida, 32310, United States*; orcid.org/0000-0002-3819-0992; Email: dhallinan@eng.famu.fsu.edu

Authors

Nam Nguyen – *Department of Chemistry and Biochemistry, Florida State University, Tallahassee, Florida 32306-4390, United States;* orcid.org/0000-0001-8424-2450

Michael P. Blatt – *Department of Chemical and Biomedical Engineering, Florida A&M University–Florida State University (FAMU-FSU) College of Engineering, 2525 Pottsdamer Street, Tallahassee, Florida, 32310, United States*; orcid.org/0000-0002-7870-2665

Kyoungmin Kim – *Department of Chemical and Biomedical Engineering, Florida A&M University–Florida State University (FAMU-FSU) College of Engineering, 2525 Pottsdamer Street, Tallahassee, Florida, 32310, United States*.

Notes

The authors declare no competing financial interest.

ACKNOWLEDGMENTS

This work was funded by the National Science Foundation under award number 1804871. The authors gratefully acknowledge Stephanie Marxsen and Prof. Rufina Alamo for insightful discussions and assistance with DSC and optical microscopy experiments.

REFERENCES

(1) Feng, X.; Ouyang, M.; Liu, X.; Lu, L.; Xia, Y.; He, X. Thermal runaway mechanism of lithium ion battery for electric vehicles: A review. *Energy Storage Mater.* **2018,** *10*, 246-267.
(2) Goodenough, J. B.; Kim, Y. Challenges for Rechargeable Li Batteries. *Chem. Mater.* **2010,** *22*, 587-603.
(3) Zhang, X. R.; Kostecki, R.; Richardson, T. J.; Pugh, J. K.; Ross, P. N. Electrochemical and infrared studies of the reduction of organic carbonates. *J. Electrochem. Soc.* **2001,** *148*, A1341-A1345.
(4) Egashira, M.; Takahashi, H.; Okada, S.; Yamaki, J.-i. Measurement of the electrochemical oxidation of organic electrolytes used in lithium batteries by microelectrode. *J. Power Sources* **2001,** *92*, 267-271.
(5) Choudhury, S.; Agrawal, A.; Wei, S.; Jeng, E.; Archer, L. A. Hybrid Hairy Nanoparticle Electrolytes Stabilizing Lithium Metal Batteries. *Chem. Mater.* **2016,** *28*, 2147-2157.
(6) He, Y.; Wang, J.; Zhang, Y.; Huo, S.; Zeng, D.; Lu, Y.; Liu, Z.; Wang, D.; Cheng, H. Effectively suppressing lithium dendrite growth via an es-LiSPCE single-ion conducting nano fiber membrane. *J. Mater. Chem. A* **2020,** *8*, 2518-2528.
(7) Glynos, E.; Pantazidis, C.; Sakellariou, G. Designing All-Polymer Nanostructured Solid Electrolytes: Advances and Prospects. *ACS Omega* **2020,** *5*, 2531-2540.
(8) Hallinan, D. T., Jr.; Balsara, N. P., Polymer Electrolytes. In *Annu. Rev. Mater. Res.*, Clarke, D. R., Ed. 2013; Vol. 43.
(9) Strauss, E.; Menkin, S.; Golodnitsky, D. On the way to high-conductivity single lithium-ion conductors. *J. Solid State Electrochem.* **2017,** *21*, 1879-1905.
(10) Meng, N.; Lian, F.; Cui, G. Macromolecular Design of Lithium Conductive Polymer as Electrolyte for Solid-State Lithium Batteries. *Small* **2021,** *17*, 2005762.
(11) Hallinan, D. T.; Villaluenga, I.; Balsara, N. P. Polymer and composite electrolytes. *MRS Bull.* **2018,** *43*, 759-767.
(12) Peng, B.; Chu, X.; Li, Y.; Li, D.; Chen, Y.; Zhao, J. Adsorption kinetics and stability of poly(ethylene oxide)-block-polystyrene micelles on polystyrene surface. *Polymer* **2013,** *54*, 5779-5789.
(13) Pesko, D. M.; Webb, M. A.; Jung, Y.; Zheng, Q.; Miller, T. F.; Coates, G. W.; Balsara, N. P. Universal Relationship between Conductivity and Solvation-Site Connectivity in Ether-Based Polymer Electrolytes. *Macromolecules* **2016,** *49*, 5244-5255.
(14) Zhang, S. S.; Xu, K.; Jow, T. R. A new approach toward improved low temperature performance of Li-ion battery. *Electrochem. Commun.* **2002,** *4*, 928-932.
(15) Li, Z.; Huang, J.; Yann Liaw, B.; Metzler, V.; Zhang, J. A review of lithium deposition in lithium-ion and lithium metal secondary batteries. *J. Power Sources* **2014,** *254*, 168-182.

(16) Liu, Y. Y.; Lin, D. C.; Yuen, P. Y.; Liu, K.; Xie, J.; Dauskardt, R. H.; Cui, Y. An Artificial Solid Electrolyte Interphase with High Li-Ion Conductivity, Mechanical Strength, and Flexibility for Stable Lithium Metal Anodes. *Adv. Mater.* **2017,** *29*, 8.
(17) Xu, W.; Wang, J.; Ding, F.; Chen, X.; Nasybulin, E.; Zhang, Y.; Zhang, J.-G. Lithium metal anodes for rechargeable batteries. *Energy Environ. Sci.* **2014,** *7*, 513-537.
(18) Barai, P.; Higa, K.; Srinivasan, V. Lithium dendrite growth mechanisms in polymer electrolytes and prevention strategies. *Phys. Chem. Chem. Phys.* **2017,** *19*, 20493-20505.
(19) Dolle, M.; Sannier, L.; Beaudoin, B.; Trentin, M.; Tarascon, J. M. Live scanning electron microscope observations of dendritic growth in lithium/polymer cells. *ECS Solid State Lett.* **2002,** *5*, A286-A289.
(20) Rosso, M.; Brissot, C.; Teyssot, A.; Dolle, M.; Sannier, L.; Tarascon, J.-M.; Bouchetc, R.; Lascaud, S. Dendrite short-circuit and fuse effect on Li/polymer/Li cells. *Electrochim. Acta* **2006,** *51*, 5334-5340.
(21) Zhang, H.; Li, C.; Piszcz, M.; Coya, E.; Rojo, T.; Rodriguez-Martinez, L. M.; Armand, M.; Zhou, Z. Single lithium-ion conducting solid polymer electrolytes: advances and perspectives. *Chem. Soc. Rev.* **2017,** *46*, 797-815.
(22) Bard, A. J.; Faulkner, L. R., *Electrochemical methods : fundamentals and applications*. 2nd ed.; Wiley: New York, 2001.
(23) Newman, J. S.; Thomas-Alyea, K. E., *Electrochemical systems*. 3rd ed.; Wiley: Hoboken, N.J., 2004.
(24) Blatt, M. P.; Hallinan, D. T. Polymer Blend Electrolytes for Batteries and Beyond. *Ind. Eng. Chem. Res.* **2021**.
(25) Young, R. J.; Lovell, P. A., *Introduction to polymers*. 3rd ed.; CRC Press: Boca Raton, 2011.
(26) Doyle, R. P.; Chen, X.; Macrae, M.; Srungavarapu, A.; Smith, L. J.; Gopinadhan, M.; Osuji, C. O.; Granados-Focil, S. Poly(ethylenimine)-Based Polymer Blends as Single-Ion Lithium Conductors. *Macromolecules* **2014,** *47*, 3401-3408.
(27) Ma, Q.; Xia, Y.; Feng, W.; Nie, J.; Hu, Y.-S.; Li, H.; Huang, X.; Chen, L.; Armand, M.; Zhou, Z. Impact of the functional group in the polyanion of single lithium-ion conducting polymer electrolytes on the stability of lithium metal electrodes. *RSC Adv.* **2016,** *6*, 32454-32461.
(28) Olmedo-Martínez, J. L.; Porcarelli, L.; Alegría, Á.; Mecerreyes, D.; Müller, A. J. High Lithium Conductivity of Miscible Poly(ethylene oxide)/Methacrylic Sulfonamide Anionic Polyelectrolyte Polymer Blends. *Macromolecules* **2020,** *53*, 4442-4453.
(29) Piszcz, M.; Garcia-Calvo, O.; Oteo, U.; del Amo, J. M. L.; Li, C. M.; Rodriguez-Martinez, L. M.; Ben Youcef, H.; Lago, N.; Thielen, J.; Armand, M. New Single Ion Conducting Blend Based on PEO and PA-LiTFSI. *Electrochim. Acta* **2017,** *255*, 48-54.
(30) Meziane, R.; Bonnet, J.-P.; Courty, M.; Djellab, K.; Armand, M. Single-ion polymer electrolytes based on a delocalized polyanion for lithium batteries. *Electrochim. Acta* **2011,** *57*, 14-19.
(31) Neary, W. J.; Kennemur, J. G. A Precision Ethylene-Styrene Copolymer with High Styrene Content from Ring-Opening Metathesis Polymerization of 4-Phenylcyclopentene. *Macromol. Rapid Commun.* **2016,** *37*, 975-979.
(32) Kieber, R. J.; Neary, W. J.; Kennemur, J. G. Viscoelastic, Mechanical, and Glasstomeric Properties of Precision Polyolefins Containing a Phenyl Branch at Every Five Carbons. *Ind. Eng. Chem. Res.* **2018,** *57*, 4916-4922.

(33) Kendrick, A.; Neary, W. J.; Delgado, J. D.; Bohlmann, M.; Kennemur, J. G. Precision Polyelectrolytes with Phenylsulfonic Acid Branches at Every Five Carbons. *Macromol. Rapid Commun.* **2018,** *39*, 1800145.
(34) Paren, B. A.; Thurston, B. A.; Neary, W. J.; Kendrick, A.; Kennemur, J. G.; Stevens, M. J.; Frischknecht, A. L.; Winey, K. I. Percolated Ionic Aggregate Morphologies and Decoupled Ion Transport in Precise Sulfonated Polymers Synthesized by Ring-Opening Metathesis Polymerization. *Macromolecules* **2020,** *53*, 8960-8973.
(35) Kim, K.; Nguyen, N.; Marxsen, S. F.; Smith, S.; Alamo, R. G.; Kennemur, J. G.; Hallinan Jr., D. T. Ionic Transport and Thermodynamic Interaction in Precision Polymer Blend Electrolytes for Lithium Batteries. *Macromol. Chem. Phys.* **2021,** *222*, 2100269.
(36) Rojas, A. A.; Inceoglu, S.; Mackay, N. G.; Thelen, J. L.; Devaux, D.; Stone, G. M.; Balsara, N. P. Effect of Lithium-Ion Concentration on Morphology and Ion Transport in Single-Ion-Conducting Block Copolymer Electrolytes. *Macromolecules* **2015,** *48*, 6589-6595.
(37) Kim, K.; Kuhn, L.; Alabugin, I. V.; Hallinan, D. T. Lithium Salt Dissociation in Diblock Copolymer Electrolyte Using Fourier Transform Infrared Spectroscopy. *Front. Energy Res.* **2020,** *8*, 240.
(38) Min, J.; Jung, H. Y.; Jeong, S.; Lee, B.; Son, C. Y.; Park, M. J. Enhancing ion transport in charged block copolymers by stabilizing low symmetry morphology: Electrostatic control of interfaces. *Proc. Natl. Acad. Sci. U.S.A.* **2021,** *118*, e2107987118.
(39) Ma, Q.; Zhang, H.; Zhou, C.; Zheng, L.; Cheng, P.; Nie, J.; Feng, W.; Hu, Y.-S.; Li, H.; Huang, X.; Chen, L.; Armand, M.; Zhou, Z. Single Lithium-Ion Conducting Polymer Electrolytes Based on a Super-Delocalized Polyanion. *Angew. Chem. Int. Ed.* **2016,** *55*, 2521-2525.
(40) Inceoglu, S.; Rojas, A. A.; Devaux, D.; Chen, X. C.; Stone, G. M.; Balsara, N. P. Morphology–Conductivity Relationship of Single-Ion-Conducting Block Copolymer Electrolytes for Lithium Batteries. *ACS Macro Lett.* **2014,** *3*, 510-514.
(41) Bocharova, V.; Wojnarowska, Z.; Cao, P.-F.; Fu, Y.; Kumar, R.; Li, B.; Novikov, V. N.; Zhao, S.; Kisliuk, A.; Saito, T.; Mays, J. W.; Sumpter, B. G.; Sokolov, A. P. Influence of Chain Rigidity and Dielectric Constant on the Glass Transition Temperature in Polymerized Ionic Liquids. *J. Phys. Chem. B* **2017,** *121*, 11511-11519.
(42) Cao, P.-F.; Wojnarowska, Z.; Hong, T.; Carroll, B.; Li, B.; Feng, H.; Parsons, L.; Wang, W.; Lokitz, B. S.; Cheng, S.; Bocharova, V.; Sokolov, A. P.; Saito, T. A star-shaped single lithium-ion conducting copolymer by grafting a POSS nanoparticle. *Polymer* **2017,** *124*, 117-127.
(43) Liu, J.; Pickett, P. D.; Park, B.; Upadhyay, S. P.; Orski, S. V.; Schaefer, J. L. Non-solvating, side-chain polymer electrolytes as lithium single-ion conductors: synthesis and ion transport characterization. *Polym. Chem.* **2020,** *11*, 461-471.
(44) Kwei, T. K. The effect of hydrogen bonding on the glass transition temperatures of polymer mixtures. *J. Polym. Sci.: Polym. Lett. Ed.* **1984,** *22*, 307-313.
(45) Kim, H. J.; Peng, X.; Shin, Y.; Hillmyer, M. A.; Ellison, C. J. Blend Miscibility of Poly(ethylene terephthalate) and Aromatic Polyesters from Salicylic Acid. *J. Phys. Chem. B* **2021,** *125*, 450-460.
(46) Polu, A. R.; Rhee, H.-W.; Kim, D. K. New solid polymer electrolytes (PEO20–LiTDI–SN) for lithium batteries: structural, thermal and ionic conductivity studies. *J. Mater. Sci: Mater. Electron.* **2015,** *26*, 8548-8554.

(47) Salmon, E.; Guinot, S.; Godet, M.; Fauvarque, J. F. Structural characterization of new poly(ethylene oxide)-based alkaline solid polymer electrolytes. *J. Appl. Polym. Sci.* **1997,** *65*, 601-607.
(48) Zardalidis, G.; Mars, J.; Allgaier, J.; Mezger, M.; Richter, D.; Floudas, G. Influence of chain topology on polymer crystallization: poly(ethylene oxide) (PEO) rings vs. linear chains. *Soft Matter* **2016,** *12*, 8124-8134.
(49) Edman, L.; Ferry, A.; Doeff, M. M. Slow recrystallization in the polymer electrolyte system poly(ethylene oxide)n–LiN(CF3SO2)2. *Journal of Materials Research* **2011,** *15*, 1950-1954.
(50) Kuo, S. W.; Chang, F. C. Miscibility and Hydrogen Bonding in Blends of Poly(vinylphenol-co-methyl methacrylate) with Poly(ethylene oxide). *Macromolecules* **2001,** *34*, 4089-4097.
(51) Mandal, T. K.; Kuo, J. F.; Woo, E. M. Miscibility and spherulite growth kinetics in the poly(ethylene oxide)/poly(benzyl methacrylate) system. *J. Polym. Sci., Part B: Polym. Phys.* **2000,** *38*, 562-572.
(52) Lodge, T. P.; Wood, E. R.; Haley, J. C. Two calorimetric glass transitions do not necessarily indicate immiscibility: The case of PEO/PMMA. *J. Polym. Sci., Part B: Polym. Phys.* **2006,** *44*, 756-763.
(53) Kennemur, J. G.; Hillmyer, M. A.; Bates, F. S. Synthesis, Thermodynamics, and Dynamics of Poly(4-tert-butylstyrene-b-methyl methacrylate). *Macromolecules* **2012,** *45*, 7228-7236.
(54) Sing, C. E.; Olvera de la Cruz, M. Polyelectrolyte Blends and Nontrivial Behavior in Effective Flory–Huggins Parameters. *ACS Macro Lett.* **2014,** *3*, 698-702.
(55) Sing, C. E.; Zwanikken, J. W.; de la Cruz, M. O. Theory of melt polyelectrolyte blends and block copolymers: Phase behavior, surface tension, and microphase periodicity. *J. Chem. Phys.* **2015,** *142*, 034902.
(56) Sing, C. E.; Zwanikken, J. W.; Olvera de la Cruz, M. Ion Correlation-Induced Phase Separation in Polyelectrolyte Blends. *ACS Macro Lett.* **2013,** *2*, 1042-1046.
(57) Marzantowicz, M.; Dygas, J. R.; Krok, F.; Lasinska, A.; Florjanczyk, Z.; Zygadlo-Monikowska, E.; Affek, A. Crystallization and melting of PEO : LiTFST polymer electrolytes investigated simultaneously by impedance spectroscopy and polarizing microscopy. *Electrochim. Acta* **2005,** *50*, 3969-3977.
(58) Xue, Z.; He, D.; Xie, X. Poly(ethylene oxide)-based electrolytes for lithium-ion batteries. *J. Mater. Chem. A* **2015,** *3*, 19218-19253.
(59) Zhou, D.; Shanmukaraj, D.; Tkacheva, A.; Armand, M.; Wang, G. Polymer Electrolytes for Lithium-Based Batteries: Advances and Prospects. *Chem* **2019,** *5*, 2326-2352.
(60) Minelli, M.; Baschetti, M. G.; Hallinan, D. T., Jr.; Balsara, N. P. Study of gas permeabilities through polystyrene-block-poly(ethylene oxide) copolymers. *J. Membrane Sci.* **2013,** *432*, 83-89.
(61) Pesko, D. M.; Feng, Z.; Sawhney, S.; Newman, J.; Srinivasan, V.; Balsara, N. P. Comparing Cycling Characteristics of Symmetric Lithium-Polymer-Lithium Cells with Theoretical Predictions. *J. Electrochem. Soc.* **2018,** *165*, A3186-A3194.
(62) Teran, A. A.; Tang, M. H.; Mullin, S. A.; Balsara, N. P. Effect of molecular weight on conductivity of polymer electrolytes. *Solid State Ionics* **2011,** *203*, 18-21.

(63) Gorecki, W.; Jeannin, M.; Belorizky, E.; Roux, C.; Armand, M. Physical properties of solid polymer electrolyte PEO(LiTFSI) complexes. *Journal of Physics: Condensed Matter* **1995,** *7*, 6823-6832.
(64) Pożyczka, K.; Marzantowicz, M.; Dygas, J. R.; Krok, F. IONIC CONDUCTIVITY AND LITHIUM TRANSFERENCE NUMBER OF POLY(ETHYLENE OXIDE):LiTFSI SYSTEM. *Electrochim. Acta* **2017,** *227*, 127-135.
(65) Georén, P.; Lindbergh, G. Characterisation and modelling of the transport properties in lithium battery polymer electrolytes. *Electrochim. Acta* **2001,** *47*, 577-587.
(66) Ma, Y.; Doyle, M.; Fuller, T. F.; Doeff, M. M.; De Jonghe, L. C.; Newman, J. The Measurement of a Complete Set of Transport Properties for a Concentrated Solid Polymer Electrolyte Solution. *J. Electrochem. Soc.* **1995,** *142*, 1859-1868.
(67) Chintapalli, M.; Le, T. N. P.; Venkatesan, N. R.; Mackay, N. G.; Rojas, A. A.; Thelen, J. L.; Chen, X. C.; Devaux, D.; Balsara, N. P. Structure and Ionic Conductivity of Polystyrene-block-poly(ethylene oxide) Electrolytes in the High Salt Concentration Limit. *Macromolecules* **2016,** *49*, 1770-1780.
(68) Pesko, D. M.; Sawhney, S.; Newman, J.; Balsara, N. P. Comparing Two Electrochemical Approaches for Measuring Transference Numbers in Concentrated Electrolytes. *J. Electrochem. Soc.* **2018,** *165*, A3014-A3021.
(69) Pesko, D. M.; Timachova, K.; Bhattacharya, R.; Smith, M. C.; Villaluenga, I.; Newman, J.; Balsara, N. P. Negative Transference Numbers in Poly(ethylene oxide)-Based Electrolytes. *J. Electrochem. Soc.* **2017,** *164*, E3569-E3575.
(70) Zugmann, S.; Fleischmann, M.; Amereller, M.; Gschwind, R. M.; Wiemhofer, H. D.; Gores, H. J. Measurement of transference numbers for lithium ion electrolytes via four different methods, a comparative study. *Electrochim. Acta* **2011,** *56*, 3926-3933.